High-Density Optical Data Storage Enabled by the Photonic Nanojet from a Dielectric Microsphere

Soon-Cheol Kong*, Alan V. Sahakian, Allen Taflove, and Vadim Backman[1]

Department of Electrical Engineering and Computer Science, Northwestern University, Evanston, IL 60208, U.S.A.
[1]*Department of Biomedical Engineering, Northwestern University, Evanston, IL 60208, U.S.A.*

Received September 2, 2008; revised November 21, 2008; accepted November 30, 2008; published online March 23, 2009

We discuss the usage of the photonic nanojet to detect deeply subwavelength pits in a metal substrate for the purpose of high-density optical data storage. Three-dimensional finite-difference time-domain (FDTD) computational solutions of Maxwell's equations are used to analyze and design the system. We find that nanojet-illuminated pits having lateral dimensions of only 100 × 150 nm^2 yield a 40-dB contrast ratio. The FDTD simulation results show that pit-depth modulation and pit-width modulation can significantly increase the optical data-storage capacity. © 2009 The Japan Society of Applied Physics

DOI: 10.1143/JJAP.48.03A008

Lossless dielectric cylinders and spheres under electromagnetic wave illumination can generate a narrow, high-intensity beam which has been called the *photonic nanojet*.[1)] The photonic nanojet was initially predicted using numerical modeling[1)] and later directly imaged at an optical wavelength.[2)] The nanojet propagates into the background medium from the shadow-side surface of a transparent dielectric cylinder or sphere of radius greater than the illuminating wavelength (λ). It appears for a wide range of diameters of the cylinder or sphere if the refractive index contrast relative to the surrounding medium is less than about 2 : 1.[3)]

The photonic nanojet is *not* an evanescent wave, despite its location in the near field of the generating cylinder or sphere. In fact, the nanojet is a propagating beam which maintains a sub-λ width for paths longer than λ if the refractive index condition is met.[3)] Furthermore, the nanojet is *not* a resonant phenomenon. In fact, its beam shape is maintained over very broad bandwidth. However, the maximum intensity of the nanojet depends upon λ and the diameter and refractive index of the cylinder or sphere. Previous numerical studies showed that the nanojet intensity can be more than 600 times the incident for a dielectric microsphere of 8 μm diameter illuminated at $\lambda = 400$ nm.[4)]

The present research was motivated by a key nanojet phenomenon — namely, inserting a tiny ($\sim\lambda/100$ diameter) particle within the nanojet perturbs the backscattered power of the lossless cylinder or sphere emitting the nanojet by an amount that is comparable to the total backscattered power of the cylinder or sphere.

Other near-field techniques have been proposed for high-density optical data-storage applications. However, these techniques generally employ evanescent waves and thus require an extremely close proximity of the read-write head and the storage medium. The length ($>\lambda$) of the photonic nanojet combined with its giant backscattering perturbation property provide relatively favorable engineering design possibilities for next-generation optical data storage.

Previous dimensionally scaled laboratory experiments at a microwave frequency (30 GHz) demonstrated the feasibility of detecting deeply subwavelength pits in a dielectric-coated metal substrate using the photonic nanojet.[5)] In this paper, we report three-dimensional finite-difference time-domain (FDTD) computational simulations with scattered-field formulation[6)] to investigate the potential use of the nanojet to detect pits in a realistic model of an optical data-storage disk. Ratios of the backscattered power with and without the pit are computed. Based upon these results, we propose a method to use the photonic nanojet to read high-density optical data.

Figure 1 illustrates the configuration studied in this paper. A 2-μm diameter polystyrene microsphere of refractive index $n = 1.59$ is assumed to be positioned 60 nm above the optical data-storage medium, which is composed of a grooved metal plate covered by a 500-nm thick dielectric layer of poly(methyl methacrylate) (PMMA). The PMMA layer thickness and the gap between the microsphere and the PMMA layer are optimized to yield the maximum detectability of a pit in the simulated data-storage disk.

In Fig. 1, the three-dimensional (3D) FDTD model employs a uniform Cartesian grid of 10-nm spatial resolution with perfectly matched layer absorbing outer grid boundaries. The metal plate is treated as a perfect electric conductor in the numerical simulation. For a source modeling, an x-polarized, modulated Gaussian impulsive plane wave propagating in the $+z$-direction is assumed. Near-field and far-field data within the spectral range of interest are obtained via discrete Fourier transformation of the transient response generated by the impulsive incident wave.

Figure 2 visualizes the FDTD-computed normalized scattered electric-field distribution in the x–z plane for a 2-μm diameter microsphere of refractive index 1.59. We observe that the focal spot is formed adjacent to the shadow-side surface of the microsphere. In this micro-optic regime where the lens dimension is not much larger than λ, the conventional formula to calculate the focal distance is not applicable.

Figure 3 graphs as a function of λ the ratio of the FDTD-computed backscattered far-field power with no pit present to the computed backscattered far-field power with the pit present. This "no-pit/pit" power ratio is generally greater than one because the pit scatters the incident nanojet and reduces the power retroreflected to the microsphere.

From Fig. 3, with a lateral (x–y plane) pit area of 100 × 150 nm^2, we observe for a pit depth of 80 nm an extremely large no-pit/pit power ratio exceeding 40 dB near $\lambda = 396.1$ nm. As the pit depth increases, the wavelength where the

*E-mail address: sch.kong@gmail.com

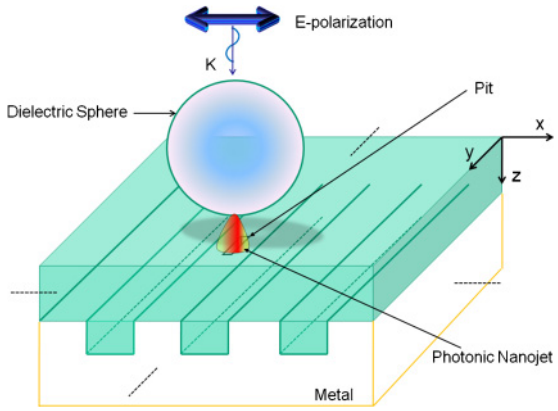

Fig. 1. (Color online) Configuration (not to scale) of the proposed optical data-storage geometry. The microsphere diameter is 2 μm. The pit width (in the *x*-direction) is 100 nm, and the pit length (in the *y*-direction) is 150 nm. The groove height (in the *z*-direction) is 40 nm; the groove periodicity is 320 nm; and 10.5 groove periods are modeled. Refractive indices for the microsphere and PMMA layer are 1.59 and 1.48, respectively.

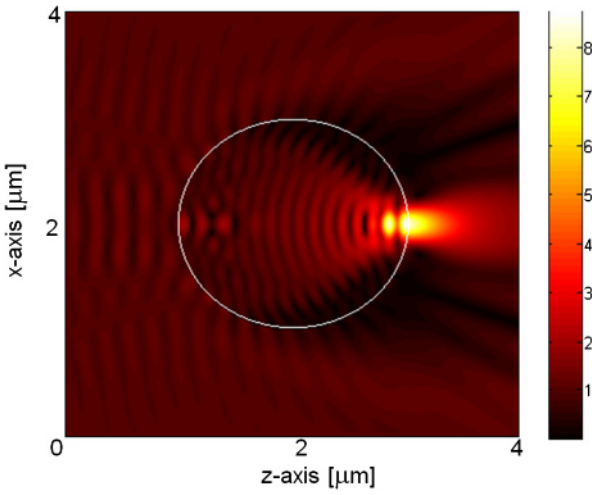

Fig. 2. (Color online) Visualization of the FDTD-computed scattered electric-field distribution in the *x*–*z* plane for a 2-μm diameter microsphere of refractive index 1.59. The values are normalized by the incident field. The incident wavelength is 400 nm.

peak occurs increases, but the opposite behavior is observed for the pit width in Fig. 3(b). We also note the no-pit/pit power ratio varies according to the pit depth and width. This property may permit the use of multi-level pit depths and/or multi-level pit widths to encode several data bits at each pit location,[7] thereby increasing the data-storage capacity and retrieval speed for a given area. Here, we show a practical example of exploiting multi-level coding by varying the pit width. Given the power ratio dependence on the pit width in Fig. 3(b), we fix the operating wavelength at 395.8 nm, and the data are replotted in Fig. 4. The monotonic nature of the reflected optical power ratio characteristic suggests a pit-width coding scheme with multiple data levels. Furthermore, the number of data bits encoded in this manner at each pit location would markedly increase as the minimum repeatable dimensional increment of pit width or depth decreases to less than 10 nm.

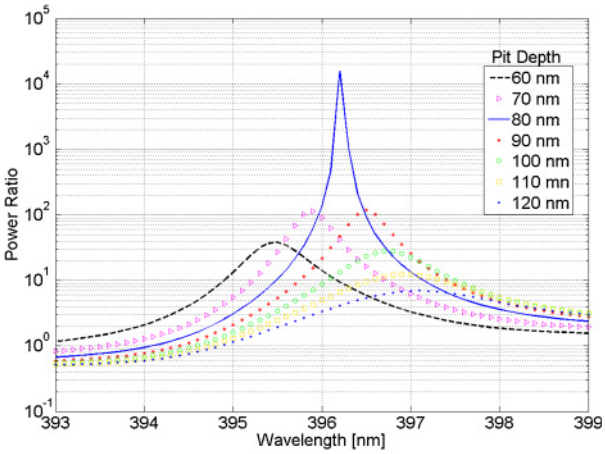

(a)

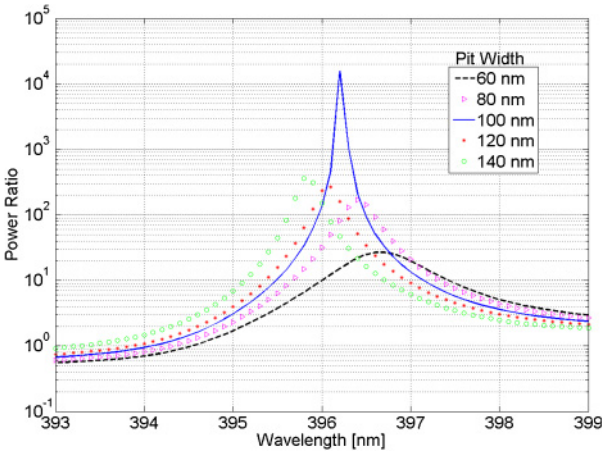

(b)

Fig. 3. (Color online) FDTD-computed far-field no-pit/pit power ratio as a function of the wavelength. (a) Pit lateral dimensions = 150 × 100 nm^2. (b) Pit length = 150 nm and pit depth = 80 nm.

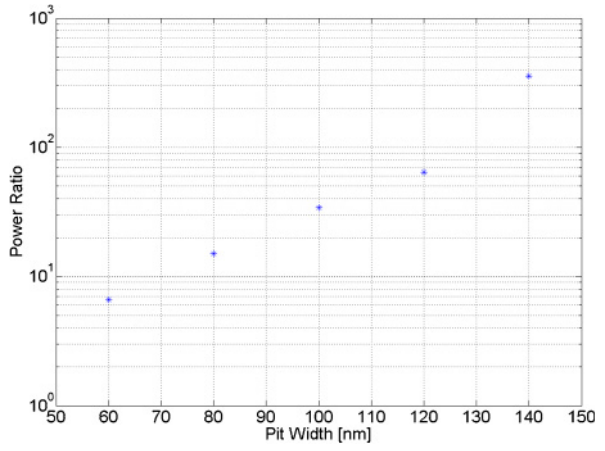

Fig. 4. (Color online) FDTD-computed far-field no-pit/pit power ratio as a function of the pit width at fixed wavelength λ = 395.8 nm. The Pit length and pit depth are set to 150 and 80 nm, respectively.

In a previous study,[7] we showed that pits having a lateral area as small as $50 \times 80\,\text{nm}^2$ can be detected using the photonic nanojet with a no-pit/pit power ratio approaching 30 dB. Furthermore, we found that a pit-to-pit separation of $\sim\lambda$ nearly eliminates crosstalk between adjacent pits. In

fact, the pit-to-pit separation distance can be used as another means to encode additional data bits due to the computed monotonic variation of the no-pit/pit power ratio with the separation between adjacent pits.

Finally, for practical implementation of the photonic nanojet technology, an ultralow refractive index aerogel could be used to mount the dielectric microsphere without impacting the characteristics of the nanojet.

In summary, we have computationally modeled the use of the photonic nanojet technique to detect a deeply subwavelength pit structure in a metal substrate for purposes of high-density optical data storage. We implemented 3D FDTD computational solutions of Maxwell's equations to design the photonic nanojet and pit configuration. The monotonic power ratios achieved using the photonic nanojet suggest the possibility of encoding several data bits at each pit according to its depth and/or width.

Acknowledgments This work was supported in part by NSF Grants CBET-0522639 and CBET-0733868. Jim Spadaro and Nikola Borisov managed and maintained Professor Backman's computer cluster.

1) Z. Chen, A. Taflove, and V. Backman: Opt. Express **12** (2004) 1214.
2) P. Ferrand, J. Wenger, A. Devilez, M. Pianta, B. Stout, N. Bonod, E. Popov, and H. Rigneault: Opt. Express **16** (2008) 6930.
3) S. Lecler, Y. Takakura, and P. Meyrueis: Opt. Lett. **30** (2005) 2641.
4) X. Li, Z. Chen, A. Taflove, and V. Backman: Opt. Express **13** (2005) 526.
5) S.-C. Kong, A. V. Sahakian, A. Heifetz, A. Taflove, and V. Backman: Appl. Phys. Lett. **92** (2008) 211102.
6) A. Taflove and S. C. Hagness: *Computational Electrodynamics: The Finite-Difference Time-Domain Method* (Artech, Boston, MA, 2005) 3rd ed., p. 220.
7) S.-C. Kong, A. V. Sahakian, A. Taflove, and V. Backman: Opt. Express **16** (2008) 13713.